J|A|C|S ARTICLES

Published on Web 01/02/2009

New Macrocyclic Terbium(III) Complex for Use in RNA Footprinting Experiments

Matthew J. Belousoff,[†,‡] Phuc Ung,[§] Craig M. Forsyth,[†] Yitzhak Tor,[*,‡] Leone Spiccia,[*,†] and Bim Graham[*,§]

School of Chemistry, Monash University, Clayton, Vic 3800, Australia, Department of Chemistry and Biochemistry, University of California, San Diego, La Jolla, California 92093-0358, and Medicinal Chemistry and Drug Action, Monash Institute of Pharmaceutical Sciences, Monash University, Parkville, Vic 3052, Australia

Received September 22, 2008; E-mail: ytor@ucsd.edu; leone.spiccia@sci.monash.edu.au; bim.graham@vcp.monash.edu.au

Abstract: Reaction of terbium triflate with a heptadentate ligand derivative of cyclen, **L1** = 2-[7-ethyl-4,10-*bis*(isopropylcarbamoylmethyl)-1,4,7,10-tetraazacyclododec-1-yl]-*N*-isopropyl-acetamide, produced a new synthetic ribonuclease, [Tb(**L1**)(OTf)(OH_2)]$(OTf)_2$·MeCN (**C1**). X-ray crystal structure analysis indicates that the terbium(III) center in **C1** is 9-coordinate, with a capped square-*anti*prism geometry. While the terbium(III) center is tightly bound by the **L1** ligand, two of the coordination sites are occupied by labile water and triflate ligands. In water, the triflate ligand is likely to be displaced, forming [Tb(**L1**)$(OH_2)_2]^{3+}$, which is able to effectively promote RNA cleavage. This complex greatly accelerates the rate of intramolecular transesterification of an activated model RNA phosphodiester, uridine-3′-*p*-nitrophenylphosphate (U*p*NP), with $k_{obs} = 5.5(1) \times 10^{-2}$ s^{-1} at 21 °C and pH 7.5, corresponding to an apparent second-order rate constant of 277(5) M^{-1}s^{-1}. By contrast, the analogous complex of an octadentate derivative of cyclen featuring only a single labile coordination site, [Tb(**L2**)(OH_2)]$(OTf)_3$ (**C2**), where **L2** = 2-[4,7,10-*tris*(isopropylcarbamoylmethyl)-1,4,7,10-tetraazacyclododec-1-yl]-*N*-isopropyl-acetamide, is inactive. [Tb(**L1**)$(OH_2)_2]^{3+}$ is also capable of hydrolyzing short transcripts of the HIV-1 transactivation response (TAR) element, HIV-1 dimerization initiation site (DIS) and ribosomal A-site, as well as formyl methionine tRNA (tRNA^{fMet}), albeit at a considerably slower rate than U*p*NP transesterification ($k_{obs} = 2.78(8) \times 10^{-5}$ s^{-1} for TAR cleavage at 37 °C, pH 6.5, corresponding to an apparent second-order rate constant of 0.56(2) M^{-1}s^{-1}). Cleavage is concentrated at the single-stranded "bulge" regions of these RNA motifs. Exploiting this selectivity, [Tb(**L1**)$(OH_2)_2]^{3+}$ was successfully employed in footprinting experiments, in which binding of the Tat peptide and neomycin B to the bulge region of the TAR stem-loop was confirmed.

Introduction

Phosphate ester bonds are an integral component of many important biological molecules, most notably DNA and RNA, and many fundamental biological processes are underpinned by reactions involving their formation or cleavage, e.g., energy storage and transfer, and cellular signaling and regulation.[1] Nature uses a complex series of enzymes (protein-based as well as ribozymes) to mediate phosphate ester condensation and hydrolysis reactions.[2] Many of these enzymes contain metal centers that are crucial to their structural integrity, or which play pivotal mechanistic roles, for example, assisting with substrate binding and activation, provision of highly reactive metal-bound nucleophiles, and stabilization of transition states and leaving groups.[2−8] By way of example, the group I intron ribozyme features multiple magnesium centers that help to neutralize the negative charge of the phosphodiester backbone and promote structure stabilization, but which also serve to coordinate the phosphodiester backbone of the exon RNA strand and activate it toward scission.[3,9]

Inspired by the occurrence of metal-containing nucleases, ribonucleases, phosphatases and ribozymes in nature, many research groups have sought to develop low-molecular weight metal complexes that are able to cleave biologically important phosphate esters.[10−19] This research has been further stimulated by the burgeoning growth in gene sequencing and genomics,

† School of Chemistry, Monash University.
‡ University of California.
§ Monash Institute of Pharmaceutical Sciences, Monash University.

(1) Lehninger, A. L.; Cox, M. M.; Nelson, D. L. *Lehninger Principles of Biochemistry*, 4th ed.; W.H. Freeman: New York, 2005.
(2) Hegg, E. L.; Burstyn, J. N. *Coord. Chem. Rev.* **1998**, *173*, 133–165.
(3) Adams, P. L.; Stahley, M. R.; Kosek, A. B.; Wang, J.; Strobel, S. A. *Nature* **2004**, *430*, 45–50.
(4) Kim, E. E.; Wyckoff, H. W. *J. Mol. Biol.* **1991**, *218*, 449–464.
(5) Strater, N.; Klabunde, T.; Tucker, P.; Witzel, H.; Krebs, B. *Science* **1995**, *268*, 1489–1492.
(6) Strater, N.; Lipscomb, W. N.; Klabunde, T.; Krebs, B. *Angew. Chem., Int. Ed.* **1996**, *35*, 2024–2055.
(7) Wilcox, D. E. *Chem. Rev.* **1996**, *96*, 2435–2458.
(8) Beese, L. S.; Steitz, J. A. *EMBO J.* **1991**, *10*, 25–33.
(9) Steitz, T. A.; Steitz, J. A. *Proc. Natl. Acad. Sci.* **1993**, *90*, 6498–6502.
(10) Sreedhara, A.; Cowan, J. A. *J. Bio. Inorg. Chem.* **2001**, *6*, 166–172.
(11) Ait-Haddou, H.; Sumaoka, J.; Wiskur, S. J.; Folmer-Andersen, J. F.; Anslyn, E. V. *Angew. Chem., Int. Ed.* **2002**, *41*, 4014–4016.
(12) Fritsky, I. O.; Ott, R.; Krämer, R. *Angew. Chem., Int. Ed.* **2000**, *39*, 3255–3258.
(13) Belousoff, M. J.; Duriska, M. B.; Graham, B.; Batten, S. R.; Moubaraki, B.; Murray, K. S.; Spiccia, L. *Inorg. Chem.* **2006**, *45*, 3746–3755.

 10.1021/ja807301r CCC: $40.75

and the realization that small, hydrolytically active metal complexes (and their conjugates with various targeting agents) may potentially find utility as robust, versatile replacements for restriction enzymes in molecular biology research, and as nucleic acid-targeting therapeutics. A number of metal complexes have already found application as so-called "conformational probes" or "footprinting reagents", used to map the structure of nucleic acids and their adducts with ligands, proteins or other nucleic acids in solution.[20−22]

Complexes of lanthanide ions have proved to be among the most effective synthetic hydrolases reported to date. The Lewis acidity of the trivalent and tetravalent lanthanide ions,[23,24] together with their high coordination numbers, fast ligand exchange rates, and absence of accessible redox chemistry, make them ideally suited to mimic the activity of the alkaline earth metal ions, Ca^{2+} and Mg^{2+}, employed by many hydrolases to bind and activate phosphate esters for cleavage. The "free" (hydrated) lanthanide ions themselves are capable of hydrolyzing a wide range of phosphate esters, including the sugar−phosphate backbone of DNA,[25−27] but are toxic and have a tendency to precipitate out of solution as hydroxides under mildly basic conditions (pH 9). Consequently, the last two decades have seen a wide variety of multidentate ligands developed to encapsulate lanthanide(III) ions in such a way as to tune and target their reactivity for biochemical applications.[28−30] Importantly, work by Hüsken and co-workers has shown that by conjugating various lanthanide complexes to an antisense oligonucleotide an antisense gene shear could be developed.[31,32]

Among the various supporting ligands that have been reported, those based on the cyclen macrocycle (1,4,7,10-tetrazacyclododecane) have featured prominently, due in large part to their ease of synthesis. The majority of these ligands are tetra-substituted derivatives featuring carboxylate, amide or alcohol pendants,[33−35] which present a total of eight coordination donors, four provided by the macrocylic amines and four by the pendant groups. While these ligands can be viewed as ideal as they form complexes which are thermodynamically stable and which exhibit greater kinetic inertness, only complexes of certain larger-sized lanthanide ions (featuring higher coordination numbers) are active as phosphate ester cleavage agents. This is because insufficient sites are left available around the smaller-sized lanthanides to allow for substrate binding and simultaneous provision of a metal-bound nucleophile.

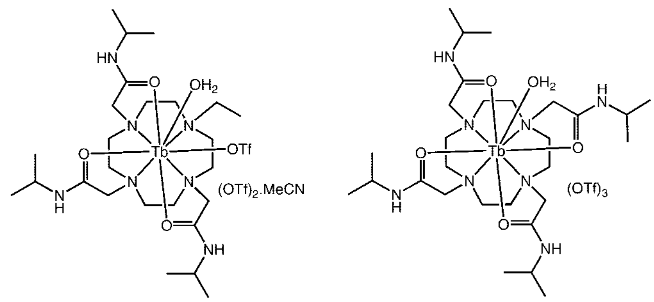

C1 **C2**

Figure 1. Terbium(III) complexes investigated in this study.

With the above in mind, we have designed a new cyclen ligand derivative, **L1** (2-[7-ethyl-4,10-*bis*(isopropylcarbamoylmethyl)-1,4,7,10-tetraazacyclododec-1-yl]-*N*-isopropyl-acetamide), with the specific objective of producing a highly active, lanthanide-based synthetic phosphate ester hydrolase. **L1** is distinguished by its three, as opposed to four, amide pendants, thus "freeing up" an additional coordination site to participate in hydrolytic reactions. Another notable feature is the presence of isopropyl groups on the amide pendants. Previous work conducted with similar tetra-substituted cyclen ligands has demonstrated that, upon lanthanide complexation, such alkyl groups produce a hydrophobic cavity that reduces the pK_a of inner-sphere coordinated water ligands to values as low as 7.[19,36] Given that metal-bound hydroxo ligands are superior nucleophiles/bases to metal-bound waters, it was envisaged that **L1** might therefore afford lanthanide complexes exhibiting improved hydrolytic activity under near physiological conditions (pH ~ 7.4). Herein, we report the synthesis of **L1**, and the crystal structure of its terbium(III) complex, [Tb(**L1**)(OTf)(OH_2)]-$(OTf)_2$·MeCN (**C1**) (Figure 1), and examine the utility of **C1** as a synthetic ribonuclease (the triflate ligand readily dissociates in aqueous solution, forming $[Tb(\mathbf{L1})(OH_2)_2]^{3+}$). Initially, we investigated the ability of the complex to accelerate cleavage of the activated phosphodiester model compound, *bis*(*p*-nitrophenyl)phosphate (BNPP), and the RNA model, uridine-3′-*p*-nitrophenylphosphate (U*p*NP). For comparative purposes, we also prepared an analogue of **C1** featuring an additional amide pendant (**C2**), but found it to be unreactive toward these substrates. The ability of $[Tb(\mathbf{L1})(OH_2)_2]^{3+}$ to promote cleavage of unactivated substrates was then probed using a series of short RNA olionucleotides—a construct of the HIV-1 transactivation response (TAR) element, a construct of the HIV-1 dimerization initiation site (DIS), and a model of the prokaryotic ribosomal

(14) Fry, F.; Fischmann, A.; Belousoff, M. J.; Spiccia, L.; Brugger, J. *Inorg. Chem.* **2005**, *44*, 941–950.
(15) Yamamoto, Y.; Uehara, A.; Tomita, T.; Komiyama, M. *Nucleic Acid. Res.* **2004**, *32*, e153/1–e153/7.
(16) Yamamoto, Y.; Uehara, A.; Watanabe, A.; Aburatani, H.; Komiyama, M. *ChemBioChem* **2006**, *7*, 673–677.
(17) Kimura, E.; Kodama, Y.; Koike, T.; Shiro, M. *J. Am. Chem. Soc.* **1995**, *117*, 8304–8311.
(18) Iranzo, O.; Kovalevsky, A. Y.; Morrow, J. R.; Richard, J. P. *J. Am. Chem. Soc.* **2003**, *125*, 1988–1993.
(19) Amin, S.; Morrow, J. R.; Lake, C. H.; Churchill, M. R. *Angew. Chem., Int. Ed.* **1994**, *33*, 773–775.
(20) Hampel, K. J.; Burke, J. M. *Methods* **2001**, *23*, 233–239.
(21) Harris, D. A.; Walter, N. G. *Curr. Protocols Nucleic Acid Chem.* **2003**, 6–8.
(22) Shcherbakova, I.; Mitra, S.; Beer, R. H.; Brenowitz, M. *Nucleic Acid. Res.* **2006**, *34*, e48.
(23) Cotton, F. A. *Advanced Inorganic Chemistry*; 6th ed.; John Wiley & Sons: New York, 1999.
(24) Lide, D. R. *CRC Handbook of Chemistry and Physics: a Ready-Reference Book of Chemical and Physical Data*, 84th ed.; CRC: Boca Raton, FL, 2003.
(25) Rishavy, M. A.; Hengge, A. C.; Cleland, W. W. *Bioorg. Chem.* **2000**, *28*, 283–292.
(26) Komiyama, M.; Takeda, N.; Shigekawa, H. *Chem. Commun.* **1999**, 1443–1451.
(27) Komiyama, M. *J. Biochem.* **1995**, *118*, 665–670.
(28) Magda, D.; Wright, M.; Crofts, S.; Lin, A.; Sessler, J. L. *J. Am. Chem. Soc.* **1997**, *119*, 6947–6948.
(29) Williams, N. H.; Takasaki, B.; Wall, M.; Chin, J. *Acc. Chem. Res.* **1999**, *32*, 485–493.
(30) Hurst, P.; Takasaki, B.; Chin, J. *J. Am. Chem. Soc.* **1996**, *118*, 9982–9983.
(31) Hüsken, D.; Goodall, G.; Blommers, M. J. J.; Jahnke, W.; Hall, J.; Häner, R.; Moser, H. E. *Biochemistry* **1996**, *35*, 16591–16600.
(32) Hall, J.; Hüsken, D.; Pieles, U.; Moser, H. E.; Häner, R. *Chem. Biol.* **1994**, *1*, 185–190.
(33) Gunnlaugsson, T.; Davies, R. J. H.; Nieuwenhuyzen, M.; O'Brian, J. E.; Stevenson, C. S.; Mulready, S. *Polyhedron* **2003**, *22*, 711–724.
(34) Gunnlaugsson, T.; O'Brian, J. E.; Mulready, S. *Tetrahedron Lett.* **2002**, *43*, 8493–8497.
(35) Morrow, J. R.; Aures, K.; Epstein, D. *Chem. Commun.* **1995**, 2431–2432.
(36) Chin, K. O. A.; Morrow, J. R. *Inorg. Chem.* **1994**, *33*, 5036–41.

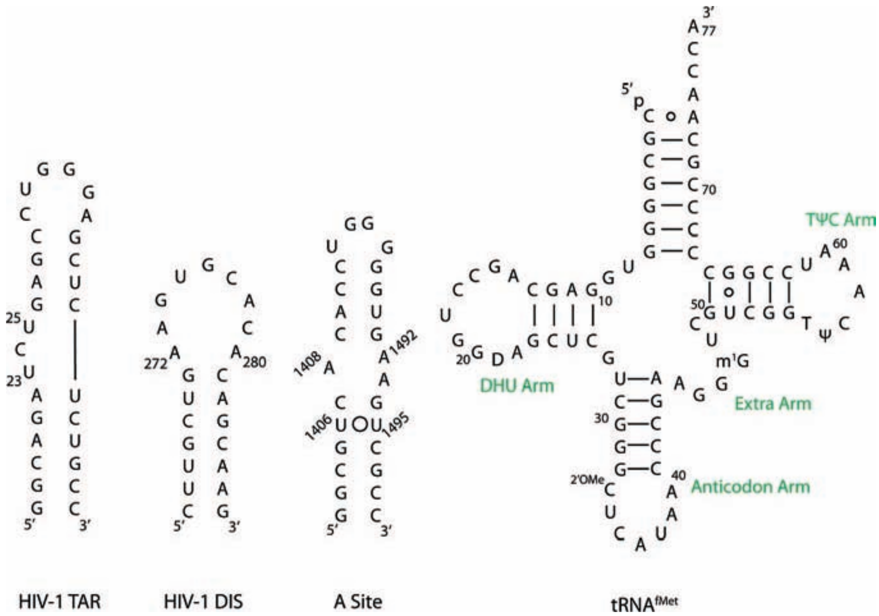

Figure 2. RNA oligonucleotides employed in this study.

A-site (A-Site), as well as the more complex, folded structure of formyl methionine tRNA (tRNA^{fMet}) (Figure 2). We found that [Tb(**L1**)(OH$_2$)$_2$]$^{3+}$ preferentially cleaves the exposed regions of these RNA motifs. This ultimately led us to explore the application of this complex as a new footprinting agent, through an examination of the changes in the metal complex-induced TAR cleavage pattern brought about by addition of the well-known TAR binders, the Tat peptide and neomycin B.

Experimental Section

Materials. All chemicals were of reagent grade quality or better, obtained from commercial suppliers and used without further purification. HPLC-grade CH_3CN and distilled H_2O were used throughout, and DMF was dried over 4 Å sieves. 1-Ethyl-1,4,7,10-tetraazacyclododecane was prepared according to a literature method.[37] Uridine-3′-*p*-nitrophenylphosphate was prepared according to a previously published procedure.[25] Custom RNA oligonucleotides were procured from Dharmacon and were deprotected using the procedure supplied by the company, then purified by PAGE gels and desalted on a Waters Corporation C-18 Sep-Pak column. Unlabeled tRNA^{fMet} was kindly donated by Prof. Simpson Joseph (Department of Chemistry and Biochemistry, University of California, San Diego). The Tat peptide (YGRKKRRNRRRP) was available from a previous study.[38]

Instrumentation. *Microanalytical* (C, H and N) analyses were performed by Campbell Microanalytical Service, Otago, New Zealand. *^{1}H NMR Spectra* were recorded in $CDCl_3$ on a Varian 300 MHz spectrometer. The chemical shifts, δ, are reported in ppm (parts per million). The abbreviations for the peak multiplicities are as follows: s (singlet), d (doublet), t (triplet), and m (multiplet). *Electrospray Mass Spectrograms* were recorded on Micromass Platform II Quadrupole Mass Spectrometer fitted with an electrospray source. A cone voltage of 20 V was used for the ligands and ligand precursor, while 70 V was used for the complexes. *UV−vis spectra* were recorded using Varian Cary 3 or 5G spectrophotometers and quartz cuvettes.

Syntheses. 2-Chloro-*N*-isopropylacetamide. A solution of chloroacetylchloride (5.48 mL, 68.9 mmol) in acetone (30 mL) was added in a dropwise fashion to a stirred, ice-cooled mixture of isopropylamine (5.86 mL, 68.2 mmol) and $Na_2CO_3 \cdot H_2O$ (8.56 g, 69.0 mmol) in H_2O (30 mL) and acetone (30 mL). The mixture was then filtered and the solvent removed under reduced pressure. The remaining residue was dissolved in CH_2Cl_2 (80 mL) and washed with 1 M HCl (2 × 40 mL), followed by 2 M $NaHCO_3$ (2 × 40 mL). After drying over $MgSO_4$, the CH_2Cl_2 was removed under reduced pressure to yield the product as a white, crystalline solid. Yield: 8.01 g, 78%. ^{1}H NMR: δ 1.26 (d, J = 6.6 Hz, 6H, CH(CH_3)$_2$), 4.07 (s, 2H, ClCH_2), 4.15 (septet, J = 6.6 Hz, 1H, CH(CH$_3$)$_2$), 6.41 (broad s, 1H, NH). ESI-MS (*m/z*): 136.1 [M+H]$^+$ (100%).

2-[7-Ethyl-4,10-bis(isopropylcarbamoylmethyl)-1,4,7,10-tetraazacyclododec-1-yl]-*N*-isopropylacetamide (L1). A stirred mixture of 2-chloro-*N*-isopropylacetamide (0.416 g, 2.74 mmol), 1-ethyl-1,4,7,10-tetraazacyclododecane (0.168 g, 0.839 mmol), $CsCO_3$ (0.967 g, 2.97 mmol) and KI (0.492 g, 2.96 mmol) in DMF (50 mL) was heated at 70 °C for 72 h. After cooling to RT, the mixture was filtered to remove inorganic salts. Removal of the solvent under reduced pressure yielded an oily brown residue, which was taken up in H_2O (30 mL) and then extracted into $CHCl_3$ (3 × 30 mL). The combined organic layers were dried over anhydrous $MgSO_4$ and the solvent removed under reduced pressure to yield a yellow oil, which was dissolved in CH_3CN (3 mL). Vapor diffusion of Et_2O into this solution yielded the product in the form of fine, white crystals. Yield: 0.171 g, 41%. ^{1}H NMR: δ 1.02 (t, J = 7.0 Hz, 3H, NCH$_2$$CH_3$), 1.16 (d, J = 6.6 Hz, 6H, CH(CH_3)$_2$), 1.20 (d, J = 6.6 Hz, 12H, CH(CH_3)$_2$), 2.03−2.65 (broad set of unresolved signals, 18H, cyclen CH_2 and NCH_2CH$_3$), 2.95−3.39 (m, 6H, NCH_2CO), 3.36 (s, 2H, NCH_2CO), 4.00 (septet, J = 6.6 Hz, 1H, CH(CH$_3$)$_2$), 4.11 (septet, 2H, CH(CH$_3$)$_2$), 6.61 (broad s, 2H, NH), 6.78 (d, J = 7.2 Hz, 1H, NH). ESI-MS (*m/z*): 250.1 [M + 2H]$^{2+}$ (100%), 498.9 [M + H]$^+$ (22%), 520.4 [M + Na]$^+$ (5%).

2-[4,7,10-tris(Isopropylcarbamoylmethyl)-1,4,7,10-tetraazacyclododec-1-yl]-*N*-isopropylacetamide (L2). A stirred mixture of 2-chloro-*N*-isopropylacetamide (1.70 g, 11.2 mmol), 1,4,7,10-tetraazacyclododecane (0.434 g, 2.52 mmol), Cs_2CO_3 (4.064 g, 12.5 mmol) and KI (2.09 g, 12.5 mmol) in DMF (50 mL) was heated at 70 °C for 48 h. After cooling to RT, the mixture was filtered to remove inorganic salts. Removal of the solvent under reduced pressure yielded an oily brown residue, which was taken up in H_2O (30 mL) and then extracted into $CHCl_3$ (3 × 30 mL). The combined organic layers were dried over anhydrous $MgSO_4$ and the solvent removed under reduced pressure to yield a yellow oil, which was

(37) Baker, W. C.; Choi, M. J.; Hill, D. C.; Thomson, J. L.; Petillo, P. A. *J. Org. Chem.* **1999**, *64*, 2683–2689.
(38) Srivatsan, S. G.; Tor, Y. *Tetrahedron* **2007**, *63*, 3601–3607.

dissolved in CH_3CN (3 mL). Vapor diffusion of Et_2O into this solution yielded the product in the form of fine, white crystals. Yield: 0.394 g, 28%. ^1H NMR: δ 1.17 (d, J = 6.6 Hz, 24H, CH(CH_3)$_2$), 2.25−2.80 (broad set of unresolved signals, 16H, cyclen CH_2), 3.09 (broad s, 8H, CH_2CO), 3.99 (heptet, J = 6.6 Hz, 4H, CH(CH_3)$_2$), 6.81 (d, J = 7.2 Hz, 4H, NH). ESI-MS (m/z): 285.6 $[M + 2H]^{2+}$ (10 0%), 569.8 $[M + H]^+$ (26%), 591.8 $[M + Na]^+$ (4%).

[Tb(L1)(OTf)(OH$_2$)](OTf)$_2$·MeCN (C1). Tb(OTf)$_3$ (0.727 g, 1.20 mmol) and **L1** (0.585 g, 1.18 mmol) were dissolved in CH_3CN (50 mL) and refluxed for 72 h. The solvent was then removed under reduced pressure to yield a brown solid, which was redissolved in CH_3CN (3 mL). Vapor diffusion of Et_2O into this solution yielded very pale yellow crystals of the product, which were suitable for X-ray crystallography. Yield: 0.906 g, 66%. Micro: *Calc* for $C_{30}H_{56}F_9N_8O_{13}S_3Tb$: C 31.0 H 4.8 N 9.6%, *Found*: C 31.0 H 4.9 N 9.7%. ESI-MS (m/z): 218.8 [Tb + **L1**]$^{3+}$ (39%), 654.7 [Tb + **L1** − 2H]$^+$ (35%), 804.6 [Tb + **L1** + OTf − H]$^+$ (100%), 954.3 [Tb + **L1** + 2OTf]$^+$ (4%).

[Tb(L2)(OH$_2$)](OTf)$_3$ (C2). Tb(OTf)$_3$ (0.270 g, 0.445 mmol) and **L2** (0.250 g, 0.440 mmol) were dissolved in CH_3CN (50 mL) and refluxed for 24 h. The solvent was then removed under reduced pressure to yield a brown solid, which was redissolved in CH_3CN (3 mL). Vapor diffusion of Et_2O into this solution yielded very pale yellow crystals of the product. Yield: 0.174 g, 33%. Micro: *Calc* for $C_{31}H_{58}F_9N_8O_{14}S_3Tb$: C 31.2 H 4.9 N 9.6%, *Found*: C 31.5 H 5.3 N 9.4%. ESI-MS (m/z): 242.7 [Tb + **L2**]$^{3+}$ (100%), 725.7 [Tb + **L2** − 2H]$^+$ (83%), 875.6 [Tb + **L2** + OTf − H]$^+$ (42%),1025.3 [Tb + **L2** + 2OTf]$^+$ (11%).

BNPP Cleavage Kinetics. A solution (total reaction volume = 2.5 mL) containing 200 μM Tb(III) complex, 50 mM MOPS buffer (pH 7.5 @ 21 °C) and 100 mM $NaClO_4$ was equilibrated at 50 °C for 20 min in a quartz cuvette (1 cm). After this time, 10 μL of a 5 mM *bis*(*p*-nitrophenyl)phosphate (BNPP) solution was added (yielding $[BNPP]_0$ = 20 μM), and the release of *p*-nitrophenoxide (NP^-) ion monitored by measuring the absorbance at 400 nm every 0.5 s for 45 min, using a UV−vis spectrophotometer. No cleavage was observed.

UpNP Cleavage Kinetics. A solution (total reaction volume = 2.5 mL) containing 200 μM Tb(III) complex, 50 mM MOPS (pH 7.5 @ 21 °C), and 150 mM $NaClO_4$ was equilibrated at the appropriate temperature for 20 min in a quartz cuvette (1 cm). After this time, 10 μL of 5 mM U*p*NP was added (yielding $[UpNP]_0$ = 20 μM), and the release of NP^- measured and modeled as a first order process, by fitting the absorbance versus time data to the equation, $Abs = A + Be^{-k_{obs}t}$, where A and B are constants.

^{32}P 5′-End-Labeling of RNA Oligonucleotides. Dephosphorylated RNA (300 pmol) was reacted with Phage T4 polynucleotide kinase (80 U) in kinase buffer (70 mM Tris.HCl (pH 7.6 @ 25 °C), 10 mM $MgCl_2$, 5 mM DTT) containing 40 μCi of γ-^{32}P-ATP (4500 C_i mmol^{-1}) and 1 mg mL^{-1} bovine serum albumin. The total volume of the reaction was 30 μL. The solution was heated at 37 °C for 1.5 h, quenched with 20 μL of loading buffer and loaded directly onto a 20% denaturing PAGE gel. The gel was imaged by autoradiography, allowing location of the product band, which was cut and extracted from the gel using 0.5 M NH_4OAc (2 × 3 mL at 55 °C for 30 min). The resulting solution was desalted using a Water C-18 Sep-Pak column. The product was then resuspended in 100 μL of H_2O, yielding a 200k cpm μL^{-1} solution of end-labeled RNA.

Cleavage of RNA Oligonucleotides. The ^{32}P end-labeled RNA oligonucleotides were refolded by slow thermal annealing, achieved by heating a 10 μM solution at 80 °C for 2 min, and then cooling the solution to 4 °C over a period of 1 h. The annealed RNA solutions were used to prepare a solution containing 1 μM RNA, 50 mM MOPS buffer (pH 6.5 @ 21 °C), 100 mM $NaClO_4$, and a varying concentration of **C1** (which forms [Tb(**L1**)(OH$_2$)$_2$]$^{3+}$ upon dissolution), to a total reaction volume of 50 μL. Control reactions containing RNA in the reaction buffer, or 2.5 μL of DMSO and the complex, were also prepared and incubated along with the other reaction mixtures. The resulting solutions were incubated at 37 °C. Five μL aliquots were periodically taken from the reaction mixture (up to 48 h), quenched with 5 μL of loading buffer (7 M urea in 10 mM Tris.HCl (pH 8.0), 100 mM EDTA and 0.05% w/v bromophenol blue), and cooled to −20 °C. The solutions were stored at this temperature until all samples had been collected. Aliquots of these stored solutions were then subjected to electrophoretic separation on a 20% denaturing PAGE gel. The developed gel was visualized by phosphorimaging and analyzed using the ImageQuant software package (Amersham Pharmacia Biotech, 2000).

Cleavage of ^{fMet}tRNA. A 10 μM solution of ^{fMet}tRNA (spiked with ^{32}P end-labeled ^{fMet}tRNA) was prepared in folding buffer (10 mM $MgCl_2$, 20 mM MOPS buffer (pH 7.0 @ 37 °C) and 100 mM $NaClO_4$). This solution was incubated at 42 °C for 30 min, to fold the tRNA, and then used directly to prepare a 50 μL solution containing 1 μM RNA, 50 or 100 μM **C1**, 50 mM MOPS buffer (pH 6.5 @ 21 °C), 1 mM $MgCl_2$ and 100 mM $NaClO_4$, which was incubated at 37 °C. Ten μL aliquots were periodically taken (up to 8 h), quenched with 10 μL of loading buffer, and cooled immediately to −20 °C. After all samples had been collected, they were subjected to electrophoretic separation on a 10% denaturing PAGE gel. The developed gel was visualized by phosphorimaging and analyzed using the ImageQuant software package.

Footprinting of TAR-Tat and TAR-Neomycin Interaction by C1. A 50 μL solution containing 1 μM TAR (spiked with ^{32}P end-labeled TAR), 100 mM $NaClO_4$, 50 mM MOPS buffer (pH 6.5 @ 21 °C) and either the Tat peptide (5−50 μM) or neomycin B (10−30 μM) was equilibrated at 37 °C for 20 min. **C1** was then added to yield a 50 μM final concentration of [Tb(**L1**)(OH$_2$)$_2$]$^{3+}$. The solution was incubated at 37 °C, with 10 μL aliquots being removed after 2−6 h, quenched with 10 μL loading buffer and cooled immediately to −20 °C. The aliquots were subjected to electrophoretic separation on a 20% denaturing PAGE gel, visualized by phosphorimaging, and analyzed using the ImageQuant software package.

X-Ray Crystallography. Intensity data were collected on a colorless crystal of **C1** (0.31 × 0.21 × 0.10 mm^3) at 123 K using a Bruker Apex II CCD fitted with graphite-monochromated Mo Kα adiation (0.71073 Å). The data were collected to a maximum 2θ value of 55° and processed using the Bruker Apex II software package. Crystal parameters and details of the data collection are summarized in Table S1 (see Supporting Information).

The crystal structure of **C1** was solved using the SHELX-97 software package,[39] and expanded using standard Fourier transform routines. All hydrogen atoms were placed in idealized positions, except the water hydrogens, which were located on the Fourier difference map. There was positional disorder for one of the isopropyl groups (containing C18, C19 and C20). The two disordered positions had the occupancies refined against each other.

Results and Discussion

Synthesis of Ligands and Terbium(III) Complexes. The two ligands employed in this study, **L1** and **L2**, were readily accessed through Finkelstein reactions between 2-chloro-*N*-isopropylacetamide and 1-ethylcylen or cyclen (Scheme 1). Formation was confirmed by ^1H NMR spectroscopy and electrospray ionization (ESI) mass spectrometry. Reaction of the ligands with Tb(OTf)$_3$ in refluxing acetonitrile yielded the corresponding terbium(III) complexes, which were crystallized as [Tb(**L1**)(OTf)(OH$_2$)](OTf)$_2$·MeCN (**C1**) and [Tb(**L2**)(OH$_2$)]-(OTf)$_3$ (**C2**), following diffusion of diethyl ether into the reaction mixtures. ESI mass spectra showed peaks corresponding to [Tb

(39) Sheldrick, G. M. *SHELXL-97*; University of Göttingen: Germany, 1997.

Scheme 1. Synthesis of Ligands **L1** and **L2**

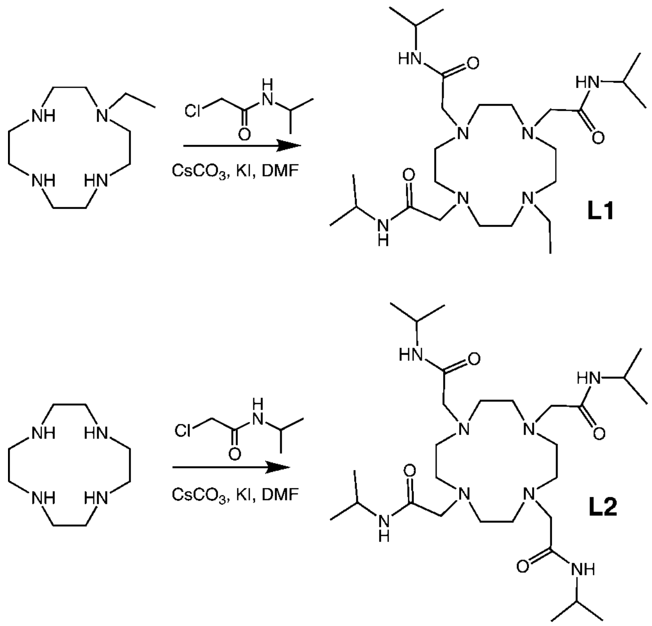

+ L]$^{3+}$, [Tb + L − 2H]$^{+}$, [Tb + L + OTf − H]$^{+}$ and [Tb + L + 2OTf]$^{+}$ (L = **L1**, **L2**), confirming formation of the complexes.

X-Ray Structure Determination. The precise molecular structure of **C1** was established by X-ray crystallography. The asymmetric unit of the triclinic ($P\bar{1}$) unit cell of **C1** contains the complex cation [Tb(**L1**)(OTf)(OH$_2$)]$^{2+}$ (Figure 3), two noncoordinated triflate anions and a cocrystallized acetonitrile molecule. The terbium(III) center is nine-coordinate, residing in a distorted, capped square-*anti*prism coordination environment (Figure 4), with the four nitrogen donors of the cyclen macrocycle occupying the basal positions of the square *anti*-prism, and three oxygens from the amide pendant arms and an *O*-coordinated triflate anion forming the "roof" of the *anti*prism. A coordinated water provides the apical cap. Importantly, the crystal structure confirms that while the terbium center in **C1** is tightly bound by **L1**, two of the coordination sites are occupied by labile ligands.

The Tb−N bonds at the base of the square vary by 0.1 Å, *c.f.* Tb(1)−N(1)/Tb(1)−N(3) (2.715(1) and 2.705(2) Å, respectively) and Tb(1)−N(2)/Tb(1)−N(4) (2.616(2) and 2.634(2) Å, respectively). This difference is also reflected in the N−Tb−N angles, which are distorted from the ideal square angle of 90° (Table S2, see Supporting Information), due to the constraints imposed by the cyclen macrocycle. The coordinated amide oxygens all share a Tb−O distance of *ca.* 2.35 Å, with the weaker coordinating triflate having a Tb−O length of 2.421(1) Å. Due to the affinity of terbium for oxygen donors, the Tb−O bond lengths are shorter on average than the Tb−N bonds by ca. 0.3 Å. Again, due to the geometric constraints of the five-membered rings formed by the coordinating amide oxygens, the N−Tb−O$_{\text{amide}}$ angles are all below the ideal 90°. The capping coordinated water has a Tb−O distance of 2.413(1) Å, and is symmetrically positioned atop the square *anti*prism, as evidenced by the fact that all of the O(1)−Tb(1)−O$_{\text{Amide/Triflate}}$ angles are around 70°. The coordination geometry, bond distances and angles found in **C1** are very similar to those found for other cyclen-based terbium(III) complexes with pendants featuring oxygen donors.[33,40−42]

Cleavage of Model Phosphate Diesters. The capacity of the two new terbium(III) complexes to cleave phosphate ester linkages was initially probed using the well-studied, activated phosphate diesters, *bis*(*p*-nitrophenyl)phosphate and (BNPP) and uridine-3′-*p*-nitrophenylphosphate (U*p*NP), which on cleavage liberate *p*-nitrophenoxide (NP^{-}), a chromophore that adsorbs at 400 nm, allowing the reaction progress to be readily monitored by UV−visible spectrophotometry. The major difference between these substrates is that U*p*NP incorporates a ribose ring with a 2′-OH group, and is thus more representative of the structure of RNA. Akin to RNA cleavage, release of NP^{-} from U*p*NP is able to proceed *via* an intramolecular transesterification mechanism, involving internal nucleophilic attack by the 2′-OH group (Scheme 2). Hydrolytic cleavage of BNPP occurs through a mechanism more closely aligned to that involved in DNA hydrolysis, for which an external nucleophile is required.

Test reactions conducted at pH 7.5, under first-order conditions (large excess of complex relative to substrate), revealed that neither **C1** nor **C2** were reactive toward BNPP, even at elevated temperature (50 °C).[43] **C2** was also found to be completely ineffectual in promoting the cleavage of U*p*NP above background (hydroxide ion-mediated) levels. In stark contrast, **C1** was found to greatly accelerate the rate of U*p*NP cleavage; 200 μM complex yielded an observed rate constant, k_{obs}, of 5.5(1) × 10^{-2} s^{-1} at 21 °C, compared to 8.25(9) × 10^{-4} s^{-1} measured in the absence of complex. This corresponds to an apparent second-order rate constant of 277(5) M^{-1}s^{-1} (a plot of k_{obs} against **C1** concentration was linear up to [complex] = 800 μM, indicating a first-order dependence of the reaction rate on **C1**). Thus, under these conditions, 1 M of complex is expected to accelerate the rate of U*p*NP cleavage by a factor of 3.4 × 10^{5} above the background rate of transesterification.

In the case of **C2**, the lack of reactivity toward both BNPP and U*p*NP can be rationalized in terms of the availability of only one labile coordination site on the terbium(III) center; substrate binding leaves no sites available for a water or hydroxo ligand that may act as a nucleophile or general base catalyst. The coordination sphere in **C1** is better suited to accommodate both monodentate substrate binding and provision of a water/hydroxide nucleophile. The inability of this complex to promote BNPP cleavage, however, suggests that the steric bulk of the **L1** ligand and BNPP prevent the **C1**-BNPP adduct from adopting a suitable conformation for direct nucleophilic attack to occur (Figure 5). Chang et al., who conducted a systematic study of the effects of various parameters on the hydrolytic activity of macrocyclic lanthanide complexes, reported that a europium(III) complex with only two inner-sphere coordinated waters was also relatively inactive as a BNPP cleavage agent.[44] U*p*NP cleavage by **C1** therefore most likely proceeds through a mechanism involving formation of a **C1**-U*p*NP adduct,

(40) Thomson, M. K.; Lough, A. J.; White, A. J. P.; Williams, D. J.; Kahwa, I. A. *Inorg. Chem.* **2003**, *42*, 4828–4841.
(41) Vojtisek, P.; Cigler, P.; Kotek, J.; Rudovsky, J.; Hermann, P.; Lukes, I. *Inorg. Chem.* **2005**, *44*, 5591–5599.
(42) Zucchi, G.; Ferrand, A.-C.; Scopelliti, R.; Bunzli, J.-C. G. *Inorg. Chem.* **2002**, *41*, 2459–2465.
(43) For simplicity we refer to the complexes present in solution as **C1** and **C2** but it should be noted that on dissolution **C1** forms [Tb(**L1**)(OH$_2$)$_2$]$^{3+}$, while **C2** forms [Tb(**L2**)(OH$_2$)]$^{3+}$.
(44) Chang, C. A.; Wu, B. H.; Kuan, B. Y. *Inorg. Chem.* **2005**, *44*, 6646–6654.

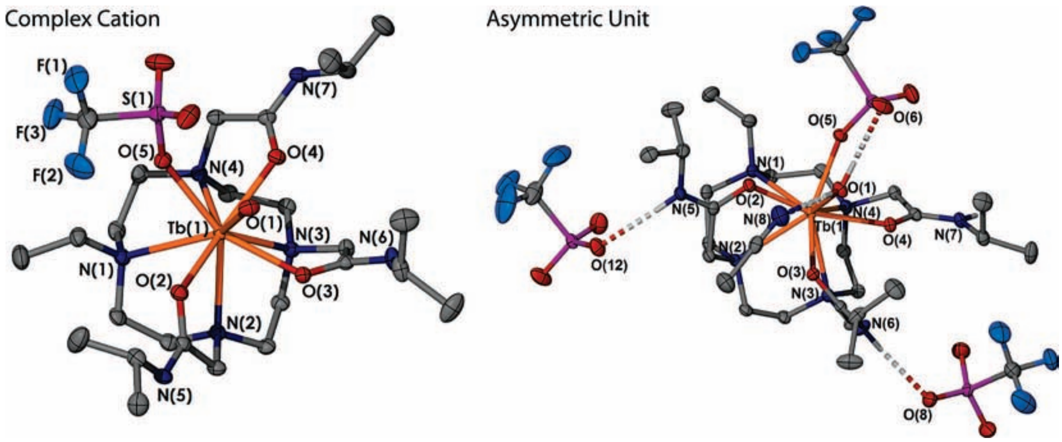

Figure 3. Thermal ellipsoid plots of the complex cation unit and the asymmetric unit of **C1** (ellipsoids drawn at 50% probability level; hydrogen atoms and the disorder about the isopropyl group (attached to N6) have been omitted for clarity; hydrogen-bonds are indicated by dashed lines).

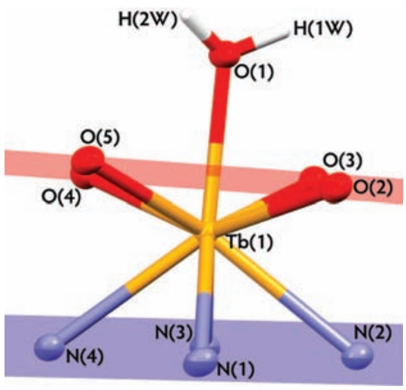

Figure 4. Thermal ellipsoid plots showing the distorted, capped square *anti*prism coordination environment about the terbium(III) center in **C1** (least-squares planes through four oxygen donors and through four nitrogen donors shown in red and blue, respectively).

Scheme 2. Mechanism for Cleavage of U*p*NP by General Base-Assisted Intramolecular Transesterification

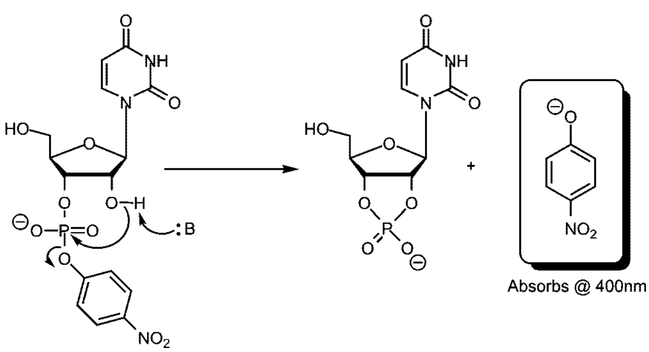

followed by internal nucleophilic attack by the 2′-OH group on the electropositive P atom. The disparate reactivity of **C1** and **C2** toward U*p*NP indicates that the terbium(III) center in **C1** is able to facilitate this transesterification step by virtue of its additional labile coordination site, conceivably through provision of a hydroxide ligand that functions as a general base catalyst in the mechanism (Figure 5). Our observations are consistent with the findings of Morrow,[19] who reported that $[LaTCMC]^{3+}$, with two inner-sphere coordinated waters, promotes hydrolysis of RNA oligomers, while two complexes with only one coordinated water, $[EuTCMC]^{3+}$ and $[DyTCMC]^{3+}$, are inactive

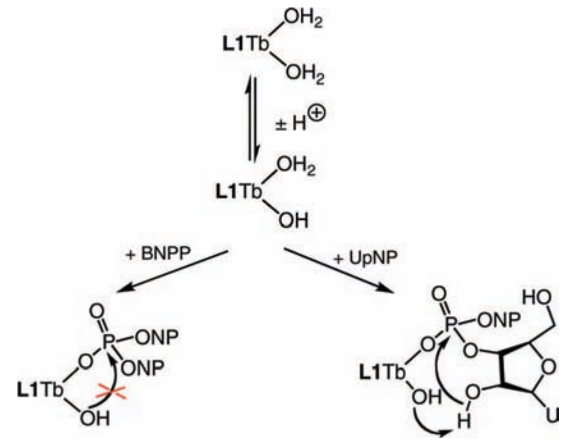

Figure 5. Proposed rationale for the disparate reactivity of **C1** toward BNPP and U*p*NP. U*p*NP features a potential internal nucleophile (2′-OH), whose reactivity may be enhanced through deprotonation by a Tb(III)-bound hydroxo group. Direct nucleophilic attack of a Tb(III)-bound hydroxo/water group on BNPP appears to be unfavorable.

(TCMC = 1,4,7,10-*tetrakis*(carbomylmethyl)-1,4,7,10-tetraazacyclododecane; this ligand is capable of octadentate coordination).

Cleavage of RNA. Encouraged by the finding that **C1** is able to greatly enhance the rate of cleavage of the RNA system model, U*p*NP, we next examined whether this complex could cleave the sugar−phosphate backbone of RNA. In the first instance, **C1** was reacted with a short ^{32}P 5′-end-labeled construct of the HIV TAR element (Figure 2) under *pseudo* first-order conditions, and the reaction mixture analyzed by polyacrylamide gel electrophoresis (PAGE) at increasing time intervals (Figure 6). Cleavage activity was evident by the appearance of several bands of lower molecular weight than the original TAR construct. Concomitant PAGE analysis of the degradation products obtained by RNase T1 digestion of the TAR construct (lane 2 of PAGE gel), located the initial scission points to be almost exclusively within the triplet base "bulge" ($U^{23}C^{24}U^{25}$) of the stem-loop structure of the construct, which NMR studies have previously shown to coincide with the position where the sugar−phosphate backbone is most exposed (Figure 6).[45] Over time, the initial cleavage fragments were

(45) Aboul-ela, F.; Varani, G.; Karn, J. *Nucleic Acid. Res.* **1996**, *24*, 3974–3981.

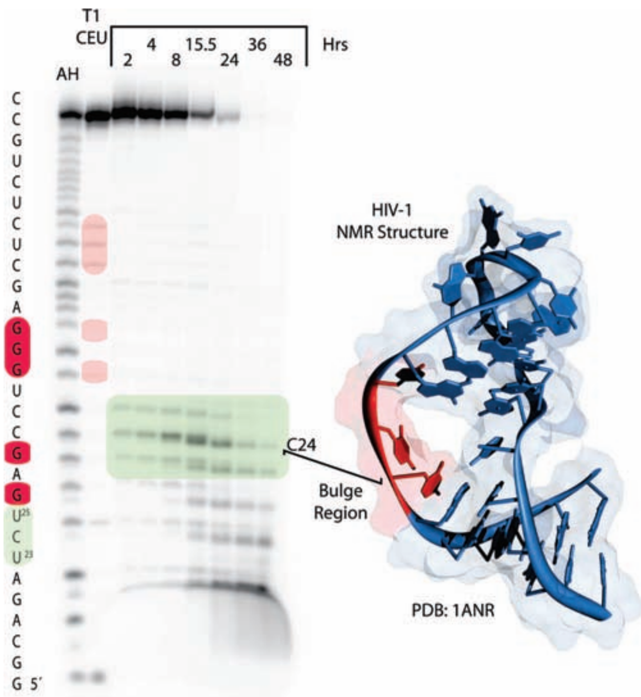

Figure 6. Phosphorimage of denaturing PAGE gel showing time dependence of cleavage of TAR construct by **C1** (lanes 3−9; incubation times indicated above lanes), together with cleavage products from alkaline hydrolysis or RNase T1 digestion (under denaturing conditions) of TAR (lanes 1 and 2, marked “AH” and “T1 CEU”, respectively). Conditions: 1 μM TAR, 50 μM **C1**, 50 mM MOPS (pH 6.5 @ 21 °C), 100 mM $NaClO_4$, 37 °C. Also shown is the NMR structure of the TAR stem-loop, highlighting the “bulge” region where **C1**-induced strand cleavage is initially focused (PDB reference: 1ANR,[45] graphic produced using UCSF Chimera[46]).

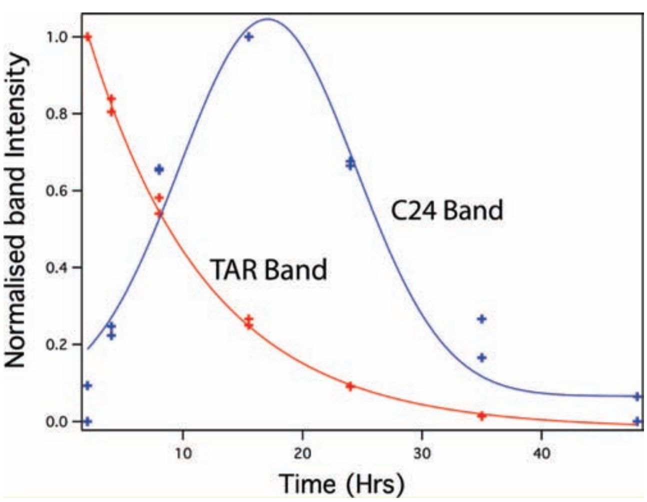

Figure 7. Plot of normalized band intensity-versus-time for the intact TAR construct as well as the major initial cleavage fragment produced *via* scission of the phosphate ester linkage adjacent to C24 after incubation with **C1**.

themselves cleaved to produce smaller secondary fragments. This was indicated by the fact that the intensities of the initial set of cleavage bands began to decrease after *ca.* 15 h (Figure 7) and coincide with the increased appearance of a set of lower molecular weight bands in the PAGE gel (Figure 6). The decrease in intensity of the band corresponding to the intact TAR construct was successfully modeled as a first-order process (Figure 7), yielding a k_{obs} value of 2.78(8) $\times$ 10^{-5} s^{-1}, corresponding to an apparent second-order rate constant of 0.56(2) $M^{-1}s^{-1}$ (under the assumption of a first-order dependence of the cleavage on the concentration of **C1**). This rate of reaction is substantially slower than that found for the transesterification of U*p*NP (*vide supra*), which is not surprising, given that the phosphate diester linkage in U*p*NP is highly activated toward cleavage because of the strongly electron-withdrawing nitrophenyl group, combined with the fact that the leaving group (NP^- ion) is highly resonance-stabilized.

Similar cleavage experiments performed with short constructs of the HIV DIS and ribosomal A-site (Figure 2) revealed that **C1** is also able to cleave the more exposed ‘solvent-exposed’ sections of the sugar−phosphate backbone of these RNA oligonucleotides (see Figure S1 in Supporting Information). This is evident by cleavage located about the unpaired adenine doublet in the A-Site construct and the $C^{280}A^{279}C^{278}$ bulge in the HIV DIS extended duplex (Figure S1, Supporting Information). In all cases, the extent of cleavage was found to be essentially the same in the presence or absence of dimethylsulfoxide (DMSO), a known radical scavenger, indicating that the cleavage reaction does not proceed through an oxidative or reductive mechanism.[47] Furthermore, the cleavage bands were found to correspond to those obtained *via* alkaline hydrolysis of the various RNA constructs, strongly supporting a transesterification/hydrolytic mechanism of cleavage (Figures 6 and S1, Supporting Information). The sites of cleavage were unaffected, and the degree of cleavage was found to be similar, over the pH range 6.0−8.5 (see Figure S2 in Supporting Information). It was also found that using a more strongly coordinating salt (NaCl, instead of $NaClO_4$) to control ionic strength led to minimal impact on cleavage efficiency. Taken together, these results indicate that **C1** is able to function as a robust synthetic ribonuclease across a reasonably broad spectrum of conditions commonly encountered in RNA manipulation/characterization studies.

The RNA cleavage properties of **C1** were further probed by examining its interaction with a more complex RNA motif, $tRNA^{fMet}$ (Figure 2), a 77-nucleotide RNA sequence that is folded into an intricate three-dimensional structure featuring a number of solvent-exposed loops. PAGE analysis of incubated mixtures of ^{32}P 5′-end-labeled $tRNA^{fMet}$ with **C1** again clearly revealed that **C1** is able to greatly accelerate RNA cleavage above the background rate (Figure 8), and that cleavage is restricted to specific sites within the RNA structure. The rate of cleavage was found to roughly double upon increasing the concentration of **C1** from 50 to 100 μM, confirming that **C1** is responsible for the observed activity. By mapping the cleavage product bands to comigrating RNase T1 digestion bands, the cleavage sites were established to be within the more exposed, single-stranded regions of $tRNA^{fMet}$, namely the DHU arm, the anticodon arm, and the extra arm (Figure 8). Correlation of these cleavage regions with the crystal structure of $tRNA^{fMet}$ as solved by Tisné and co-workers[48] clearly reveals that the strand scission induced by **C1** is located in regions where the phosphate ester backbone is more “exposed” (see Figure 8) to attack by the bulky terbium(III) complex.

(46) Pettersen, E. F.; Goddard, T. D.; Huang, C. C.; Couch, G. S.; Greenblatt, D. M.; Meng, E. C.; Ferrin, T. E. *J. Comput. Chem.* **2004**, *25*, 1605–1612.
(47) The rate of cleavage of the DIS construct appeared to be slightly higher in the presence of DMSO, which may reflect a shift in equilibrium from the more stable, extended duplex form of DIS towards the more cleavage-susceptible hairpin form in the presence of DMSO.
(48) Barraud, P.; Schmitt, E.; Mechulam, Y.; Dardel, F.; Tisne, C. *Nucleic Acid. Res.* **2008**, *36*, 4894–4901.

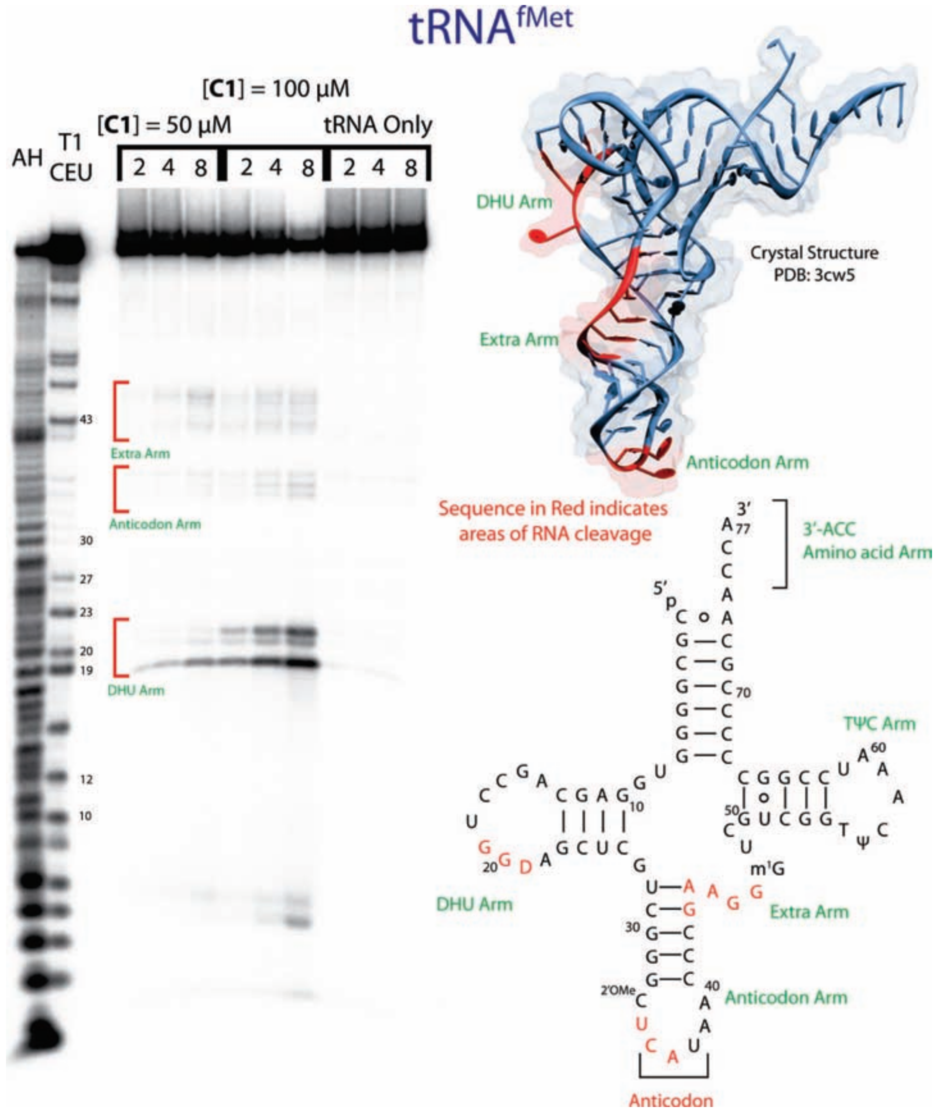

Figure 8. Phosphorimage of denaturing PAGE gel showing time dependence and concentration dependence of cleavage of ^{fMet}tRNA by **C1** (lanes 3−11), together with cleavage products from alkaline hydrolysis or RNase T1 digestion (under denaturing conditions) of TAR (lanes 1 and 2, marked "AH" and "T1 CEU", respectively). Lanes 2−4: 50 μM **C1** with ^{fMet}tRNA (2, 4, 8 h incubation time); lanes 5−7: 100 μM **C1** with ^{fMet}tRNA (2, 4, 8 h incubation time); lanes 8−10: ^{fMet}tRNA only control (2, 4, 8 h incubation time); incubation times indicated above lanes. Conditions: 1 μM ^{fMet}tRNA, 50 mM MOPS (pH 6.5 @ 21 °C), 100 mM $NaClO_4$, 1 mM $MgCl_2$, 37 °C. Shown also is the crystal structure of tRNA^{fMet} (as determined by Tisné et al.[48] (PDB: 3cw5), graphic prepared using UCSF Chimera[46]) highlighting (in red) the areas of focused strand scission induced by **C1**.

Footprinting Experiments. Having established that **C1** is able to selectively cleave solvent-exposed, single-stranded (or strained sections) of a folded RNA structure, we next explored whether **C1** could be employed as a new footprinting reagent, useful for examining the interaction between ligands and their RNA targets. RNA-ligand footprinting is often carried out using RNase enzymes, however, this can sometimes be a complex and time-consuming task (requiring case-by-case optimization), and the conditions required for enzyme activity may be incompatable with the conditions under which ligand binding occurs. Thus, robust synthetic reagents that are able to function as artificial ribonucleases under near physiological conditions represent valuable additions to the arsenal of tools used to examine RNA structure and RNA-ligand interactions. The Fe(II)−EDTA/H_2O_2 system, which is utilized to generate Fenton based hydroxide radicals, is often used for DNA and RNA footprinting,[22] but its lack of sequence specificity can be problematic.[49]

We chose the TAR construct as a model RNA target, since a great deal is known about its interactions with a range of different ligands. Figure 9 shows the cleavage "footprints" observed upon incubating **C1** with the TAR construct, both in isolation and in the presence of two known TAR-binders, the Tat peptide and neomycin B. The Tat peptide comprises the portion of the Tat protein that is involved in binding of this protein to the TAR element, an interaction that that is vital to the HIV replication cycle. It is known that the Tat peptide binds to the triplet base "bulge" region of TAR.[50] Moreover, NMR studies carried out by Crothers et al.[50] suggest that upon Tat binding, the phosphate ester groups associated with U^{23} and C^{24} become more exposed relative to that of U^{25}. Consistent with these observation/predictions, we found a change in the cleavage footprint upon addition of Tat peptide to the **C1**/TAR mixture:

(49) Pogozelski, W. K.; D., T. T. *Chem. Rev.* **1998**, *98*, 1089–1107.
(50) Long, K. S.; Crothers, D. M. *Biochemistry* **1999**, *38*, 10059–10069.

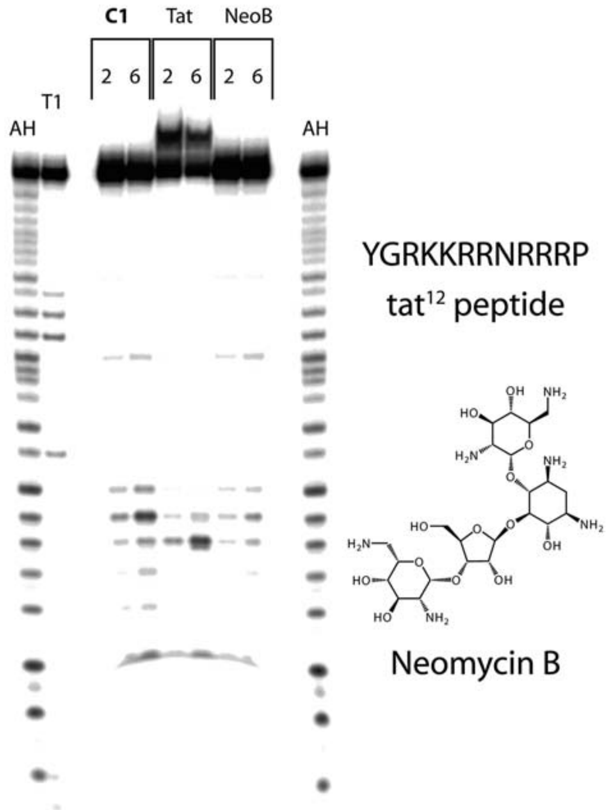

Figure 9. Phosphorimage of denaturing PAGE gel showing "footprints" for cleavage of TAR by **C1**, both in the absence and presence of Tat peptide or neomycin B. Lanes 1 and 9: alkaline hydrolysis ladder; lane 2: RNase T1 digestion of TAR (under denaturing conditions); lanes 3 and 4: **C1** with TAR (2, 6 h incubation time); lanes 4 and 5: **C1** with TAR (6 h reaction time); lanes 5 and 6: **C1** with TAR and Tat (2, 6 h incubation time); lanes 7 and 8: **C1** with TAR and neomycin B (2, 6 h incubation time); incubation times indicated above lanes. Conditions: 1 μM TAR, 50 μM **C1**, 50 mM MOPS (pH 6.5 @ 21 °C), 100 mM $NaClO_4$, 37 °C.

cleavage adjacent to U^{25} was suppressed, while cleavage adjacent to U^{23} was enhanced.

It has been postulated that the naturally occurring aminoglycoside, neomycin B, also binds the triplet base "bulge" region of TAR,[51] but that this is a more dynamic *on/off* binding interaction than for Tat. Accordingly, we found that the cleavage patterns obtained both in the absence and presence of neomycin B were very similar, but that the extent of cleavage was about 4-fold lower when neomycin B was present (cf., lanes 3 and 4 with lanes 7 and 8 in Figure 9). **C1** is thus able to detect the interaction of neomycin B with TAR, by virtue of the bound state of neomycin B providing TAR with some protection against **C1**-induced cleavage.

Conclusion

A new terbium(III) complex, **C1**, which is able to rapidly accelerate the cleavage of U*p*NP, as well as the solvent-exposed, single-stranded regions of folded RNA motifs, has been developed. The complex does not require co-reactants to cause RNA scission, is able to function over a range of pHs, and exhibits cleavage activity that is sensitive to the presence of RNA-binding ligands. **C1** is thus a suitable candidate for use in footprinting assays directed at improving our understanding of RNA structure and RNA-ligands interactions.

Acknowledgment. M.J.B. is a recipient of an Australian Post Graduate Award, a Monash University travel grant, a Monash Postgraduate Publication Award and a Fulbright Fellowship. We acknowledge the financial support of National Institutes of Health (grant numbers AI 47673 and GM 069773) (for Y.T.) and Monash University.

Supporting Information Available: X-ray crystallography refinement data tables (Table S1) and selected bond lengths and angles for **C1** (Table S2), phosphorimages of cleavage reaction of **C1** with the TAR, DIS and A-Site RNA (Figure S1) and phosphorimage of the pH dependence of the reaction of **C1** with TAR (Figure S2). This material is available free of charge via the Internet at http://pubs.acs.org.

JA807301R

(51) Faber, C.; Sticht, H.; Schweimer, K.; Rosch, P. *J. Biol. Chem.* **2000**, *275*, 20660–20666.